# Molecular Dynamics Simulations of Ribonuclease T1: Analysis of the Effect of Solvent on the Structure, Fluctuations, and Active Site of the Free Enzyme†

Alexander D. MacKerell, Jr.,* Lennart Nilsson, and Rudolf Rigler
*Department of Medical Biophysics, Karolinska Institutet, S-104 01 Stockholm, Sweden*
Wolfram Saenger
*Institute for Crystallography, Free University Berlin, Takustrasse 6, D-1000 Berlin 33, FRG*
*Received October 27, 1987; Revised Manuscript Received February 12, 1988*

ABSTRACT: Molecular dynamics simulations were performed on ribonuclease T1 (RNase T1; EC 3.1.27.3) to determine a structure for the free enzyme. Simulations starting with the X-ray coordinates for the 2′GMP–RNase T1 complex were done in vacuo and with an 18-Å water ball around the active site using stochastic boundary conditions to understand the influence of water on both the structure and fluctuations of the enzyme. Removal of 2′GMP caused structural changes in the loop regions, including those directly interacting with the bound inhibitor in the crystal structure, while regions of secondary structure were less affected. The presence of solvent in the simulation damped the structural changes observed, which may be related to the use of full charges in both simulations. Fluctuations were also affected by the water, which generally increased both at the surface and in the interior of the protein. The active site in vacuo collapsed upon itself, forming a number of protein–protein hydrogen bonds leading to larger structural changes and lowered fluctuations while the presence of water kept the active site open, minimized structural changes, and increased fluctuations. Such fluctuations in the active site may be important for the binding of inhibitors or substrates to the enzyme. Lastly, results from the water simulation allow the prediction of a motion for a hypothetical tryptophan at position 45, which can ultimately be tested experimentally via time-resolved fluorescence using a site-specific mutant of the enzyme.

Ribonuclease T1 (RNase T1;[1] EC 3.1.27.3) from *Aspergillus oryzae* is an invaluable tool in nucleic acid research due to its specific cleavage of single-stranded RNA on the 3′-side of guanosine (Egami et al., 1964; Uchida & Egami, 1971; Takahashi & Moore, 1982). This specificity of interaction also makes RNase T1 an excellent system for the study of protein–nucleic acid interactions (Egami et al., 1964; Heinemann & Saenger, 1982). Catalytically, the enzyme accelerates the cleavage of 3′–5′ phosphodiester bonds in RNA and is thought to follow a mechanism similar to that seen in RNase A (Roberts et al., 1969), where a 2′,3′-cyclic phosphate intermediate is formed, followed by hydrolysis yielding a terminal guanosine 3′-phosphate (Takahashi & Moore, 1982; Heinemann & Saenger, 1982). Residues indicated to be involved in the mechanism include His-40, Glu-58, His-92, and possibly Arg-77 (Takahashi & Moore, 1982).

Structurally, the enzyme is a monomer of $M_r$ 11 085, containing 104 amino acids. X-ray crystallographic structures are known for the 2′GMP– (Heinemann & Saenger, 1982; Sugio et al., 1985a; Arni et al., submitted for publication) and 3′GMP– (Sugio et al., 1985b) enzyme complexes showing both inhibitors to be bound in a similar fashion. The guanine moiety is bound in a stacked configuration between two tyrosine residues (42 and 45) with several specific hydrogen bonds formed with both side-chain and backbone atoms. With the phosphate moiety several hydrogen bonds are present with the side chains of residues involved in the catalytic mechanism. Concerning secondary structure, the enzyme contains one $\alpha$-helix, a $\beta$-pleated sheet, two disulfide bonds, and several loop regions (Figure 1) (Arni et al., submitted for publication). Although the structure of RNase T1 in the presence of inhibitors is known, the structure of free RNase T1, which has been crystallized (Martin et al., 1980), remains unknown.

Conformational changes are known to occur in a variety of proteins upon interaction with substrates, inhibitors, or other regulatory modifiers (Steitz et al., 1982). Spectroscopic studies on RNase T1, including time-resolved fluorescence (MacKerell et al., 1987a,b) and nuclear magnetic resonance (H. Ruterjans, personal communication), indicate the occurrence of such changes upon the binding of the inhibitors 2′GMP and 3′GMP, which may play an important role in both the specificity and the catalytic mechanism of RNase T1. To better understand the conformational changes occurring in RNase T1, a structure of the free enzyme, allowing comparison with the RNase T1–inhibitor complexes, is required.

One way to get to an "unknown" structure is by molecular dynamics (MD) simulations (Karplus & McCammon, 1981; McCammon, 1984; Warshel, 1984) starting with a similar known structure. This approach has been used previously to determine an apo structure for the retinol binding protein (Åqvist et al., 1986) by starting with the structure for the holo enzyme. The basis of this approach lies in the assumption that a dynamically stable structure, as evidenced by a structure fluctuating around a stable potential energy minimum, is

† This work was supported in Stockholm by a NATO postdoctoral fellowship from the NSF to A.D.M. and grants from the Knut and Alice Wallenberg Foundation, the Swedish Natural Science Research Council, and the Lisa and Johan Grönberg Foundation and in Berlin by the Sonderforschungsbereich 9 and by Fonds der Chemischen Industrie.
* Author to whom correspondence should be addressed at the Department of Chemistry, Harvard University, 12 Oxford St., Cambridge, MA 02138.

[1] Abbreviations: RNase T1, ribonuclease T1 (EC 3.1.27.3); 2′GMP, guanosine 2′-monophosphate; SBS, stochastic boundary simulation; VS, vacuum simulation; MD, molecular dynamics; RMS, root mean square.

0006-2960/88/0427-4547$01.50/0 

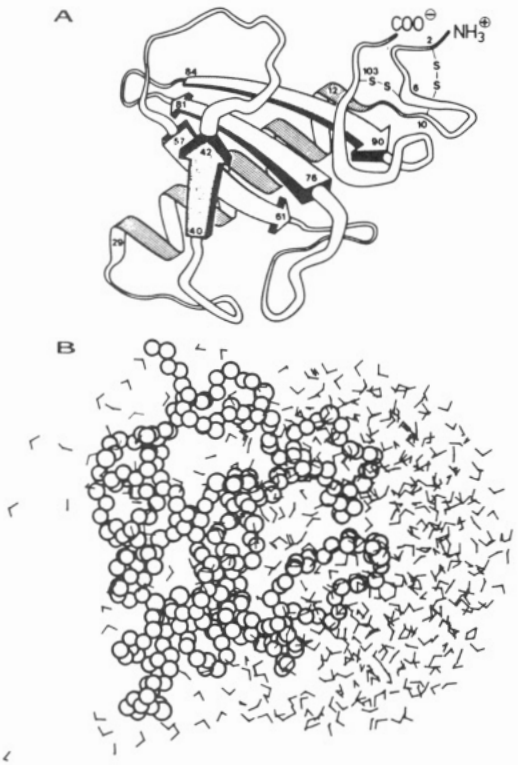


FIGURE 1: (A) Structure of ribonuclease T1 in the presence of 2′GMP [2′GMP removed; from Heinemann and Saenger (1982)]. (B) Diagram of ribonuclease T1 main-chain atoms (N, Cα, O) (circles) and water molecules (stick representation) following the initial minimization in the SBS simulation.

obtained that is locally ergodic (Palmer, 1982) within a global minimum representing the true structure. Following this assumption, simulations on RNase T1, starting with the X-ray coordinates for the RNase T1–2′GMP complex (Arni et al., unpublished results) with 2′GMP removed, were undertaken to determine a structure for the free enzyme.

A previous MD study of RNase T1 was performed on the free enzyme with emphasis on the motion of Trp-59, which showed good agreement with experimental results, and on RMS fluctuations in the enzyme (MacKerell et al., 1987b). That study, however, started with 2.5-Å resolution coordinates (Heinemann & Saenger, 1982) which have recently been refined to 1.9 Å (Arni et al., submitted for publication). Those MD results indicate the presence of relatively large fluctuations in the active-site portion of the enzyme. To understand the effect of solvent (Warshel & Levitt, 1976; Hagler & Moult, 1978; Ahlström et al., 1987) on the overall structure and the active site in particular, a simulation using a variation of the stochastic boundary approach (Adelman, 1980; Berkowitz & McCammon, 1980; Brooks & Karplus, 1983; Brunger et al., 1984, 1985; Brooks, et al., 1985; Belch & Berkowitz, 1985) allowing the incorporation of water in the active-site portion of the enzyme was undertaken in the present study. Furthermore, to allow a better comparison with results in vacuo, a simulation of the free enzyme without water was performed starting with the 1.9-Å X-ray coordinates. From these calculations the effect of water on the structure and fluctuations of RNase T1 along with a preliminary structure for free RNase T1 is reported. Comparison with the X-ray crystallographic RNase T1–2′GMP complex is also performed, though a more detailed comparison of both the fluctuations and structures of free RNase T1 and the RNase T1–2′GMP complex will be presented elsewhere (MacKerell et al., submitted for publication).

## METHODS

Molecular dynamics simulations were performed by using the program CHARMM (Brooks et al., 1983) on a NORD-500 computer. Calculations involve the determination of the forces on each atom using an empirical energy function that includes terms for bond lengths, bond angles, dihedral (torsion) angles, improper torsion angles, van der Waals interactions, and electrostatic interactions. Explicit hydrogen-bonding terms were not required as those interactions are accounted for by the van der Waals and electrostatic interactions (Reiher, 1985). Parameters for the simulations were those currently supported by CHARMM and included the use of full charges in both simulations.

Starting coordinates for the MD trajectories were the refined coordinates for the 2′GMP–RNase T1 complex at 1.9-Å resolution (Arni et al., submitted for publication). Prior to the simulations the 2′GMP atoms were removed. Coordinates for polar hydrogen atoms were determined from the standard geometric parameters (Brooks et al., 1983). For the vacuum simulation, 3 of the 91 waters identified by the X-ray crystallography (crystal waters), which fill a channel from the protein surface to Trp-59, were included. In the water simulation all of the crystal waters were included along with a bulk water sphere around the enzyme's active site (Figure 1B). The three histidine residues (27, 40, and 92) were set to a doubly protonated state with a charge of +1 to complement various experimental and structural data obtained at pH 5.3 (Heinemann & Saenger, 1982; Arni et al., submitted for publication) as well as NMR studies indicating that the histidine residues have high $pK_a$ values and are therefore protonated at pH 5.3 (Ruterjans & Pongs, 1971; Arata et al., 1979).

For the stochastic boundary simulation (SBS) the following parts of the enzyme were included in the full reaction region (Brooks et al., 1985): the active site and regions of the enzyme in which RMS fluctuations in the previous free enzyme vacuum simulation were greatest (MacKerell et al., 1987b) and where RMS differences between the RNase T1–2′GMP X-ray structure and the time-averaged free RNase T1 structure were greatest (A. D. MacKerell, Jr., unpublished results). This selection resulted in an 18-Å radius sphere around Tyr-42 OH (Figure 1B), which was filled by overlaying an 18-Å water ball of TIP3P water (Jorgensen et al., 1983) prepared from a Monte Carlo study of 216 waters using periodic boundary conditions. Following the overlaying of the water, water molecules that coincided with protein atoms were removed. The system was then partitioned into two parts, a full MD region of both protein and water atoms included in the 18-Å sphere and a Langevin region of protein and crystal water molecules outside the sphere. The partitioning was done such that all residues with at least one atom in the full MD region were included in that region (Brooks et al., 1985). Also, the three water molecules in the channel leading to Trp-59 were included in the Langevin region to allow them the freedom to move out of the channel. To maintain the water molecules within the 18-Å sphere, a constraint potential (Warshel, 1979; Warshel & Russell, 1984) was applied with a radius of 20.5 Å to account for the van der Waals radii of the water molecules. Since the whole protein was included in either the full MD region or the Langevin region, harmonic restoring forces which are normally applied to protein atoms in the Langevin region were not required. Thus, large protein fluctuations could occur through the constraining potential while the proper water density was maintained in the 18-Å sphere. Atoms in the Langevin region, where the normal full MD treatment is

supplemented by a random-force term and a frictional term, were assigned a frictional coefficient of 50 $ps^{-1}$ (Brooks et al., 1985).

Following the overlaying and partitioning of the system, the positions of the water molecules were energy minimized for 50 steepest descent steps while the protein conformation was constrained. Reorientation of the 18-Å water ball and overlaying of the 18-Å active-site sphere followed by removal of all overlapping waters were performed 4 times to ensure that the proper water density was achieved. Repartitioning of the system was then performed, yielding 2051 atoms in the full MD region and 341 atoms in the Langevin region. Partitioning of the residues into full MD and Langevin regions is shown in Figures 3C, 4A and 5A,B, where residues in the two regions are represented as circles and squares, respectively. Steepest descent minimization of the entire system was then performed for 200 steps with harmonic constraints on the protein atoms which were gradually decreased every 40 steps. For the MD run the algorithm SHAKE (Ryckaert et al., 1977; van Gunsteren & Karplus, 1982) was used to constrain all covalent bonds involving hydrogen atoms during the simulation allowing an integration time step of 0.002 ps. The electrostatic potential was shifted to obtain a gradual cutoff, as was the van der Waals potential, and a nonbonded interaction cutoff of 8.0 Å was used (Brooks et al., 1983). The molecular dynamics trajectory was initiated by instantaneously assigning the atoms with random velocities, yielding an overall kinetic energy corresponding to 300 K. Equilibration of the system was then performed for the next 16 ps with a temperature window of ±10 K and checking of the window every 100 steps (0.2 ps) with rescaling when necessary. When the simulation was continued without temperature checking, however, the temperature of the system continued to rise to approximately 330 K. At time 43 ps of the simulation the temperature of the system was rescaled to 314 K and was then maintained throughout the remainder of the trajectory by applying a temperature window of ±2 K with checking every 50 steps (0.1 ps).

Energy minimization of the X-ray structure prior to the vacuum simulation (VS) was done by using 200 adopted-basis Newton Raphson (Brooks et al., 1983) steps, following which the structure was instantaneously heated to 310 K. Equilibration was performed for 20 ps with a temperature window of ±10 K, with checking of the window every 100 steps (0.2 ps). Following the equilibration of a temperature window of ±2 K with checking every 50 steps was applied and used throughout the remainder of the simulation. The electrostatic potential was shifted to obtain a gradual cutoff, while the van der Waals potential used a switching function between 6.5 and 7.5 Å, and a nonbonded interaction cutoff of 8.0 Å was used (Brooks et al., 1983).

Analysis of the trajectories was performed by using coordinate sets selected every 0.1 ps. The portion of the trajectories used in the analysis were selected when the potential energy and the RMS difference between coordinate sets obtained from averaging the individual coordinate sets over 5.0 ps and the initial X-ray coordinates both became relatively stable (Figure 2). This selection led to time ranges of 30–160 ps for the VS and 53–176 ps for the SBS being used. RMS differences, $\Delta r$, were calculated by using

$$\Delta r = [(1/N)\sum_{i=1}^{N}(r_{i1} - r_{i2})^2]^{1/2} \quad (1)$$

where $r_{i1}$ and $r_{i2}$ are the positions being compared and the summation is over the backbone (N, Cα, C, O) or side-chain atoms (not including hydrogens and Gly O) of the individual residue or the entire protein. RMS fluctuations, $\Delta R$, were calculated by using

$$\Delta R = [(1/N)\sum_{i=1}^{N}\langle[(\Delta x_i)^2 + (\Delta y_i)^2 + (\Delta z_i)^2]\rangle]^{1/2} \quad (2)$$

where $\Delta x_i$, $\Delta y_i$, and $\Delta z_i$ are the differences between the reference and instantaneous atomic coordinates for the $i$th atom, the broken brackets ($\langle\ \rangle$) represent the time average, and the summation is over the backbone or side-chain atoms of the individual residues.

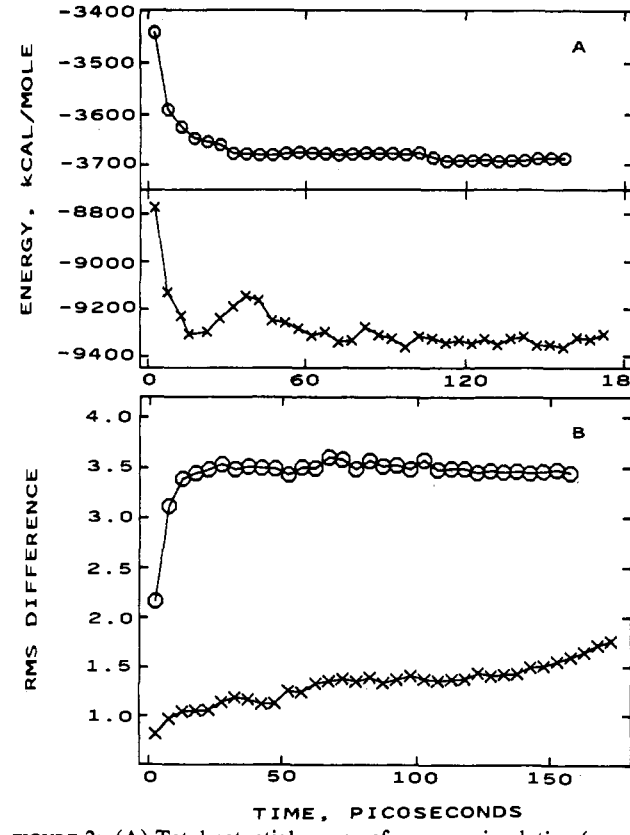


FIGURE 2: (A) Total potential energy of vacuum simulation (upper, O) and stochastic boundary simulation (lower, ×) as a function of time. (B) RMS difference between 5-ps time-averaged backbone atom (N, Cα, C, O) positions and the initial X-ray positions for the vacuum simulation (O) and stochastic boundary simulation (×).

## Results and Discussion

*Structure Stability.* Presented in Figure 2A are the changes in potential energy of the two simulations with time. In the SBS the potential energy reached a minimum at 16 ps; however, following the equilibration period and subsequent removal of temperature checking, the potential energy started to increase. The cause of this increase is currently under investigation. At 43 ps the velocities of the atoms were rescaled to a corresponding temperature of 314 K, and a ±2 K temperature window was applied to maintain the temperature throughout the remainder of the simulation. A similar temperature window was then used in the VS to allow better comparison of the two simulations. The use of this temperature maintenance appeared to have minimal effect on the overall results as compared to a previous simulation (MacKerell et al., 1987b); however, its use precludes comparison of the simulations with any of the standard thermodynamic ensembles (McCammon & Harvey, 1987).

Figure 2B shows the RMS difference between the X-ray RNase T1–2′GMP coordinates and 5-ps time-averaged coordinates for both the VS and SBS as a function of time. In

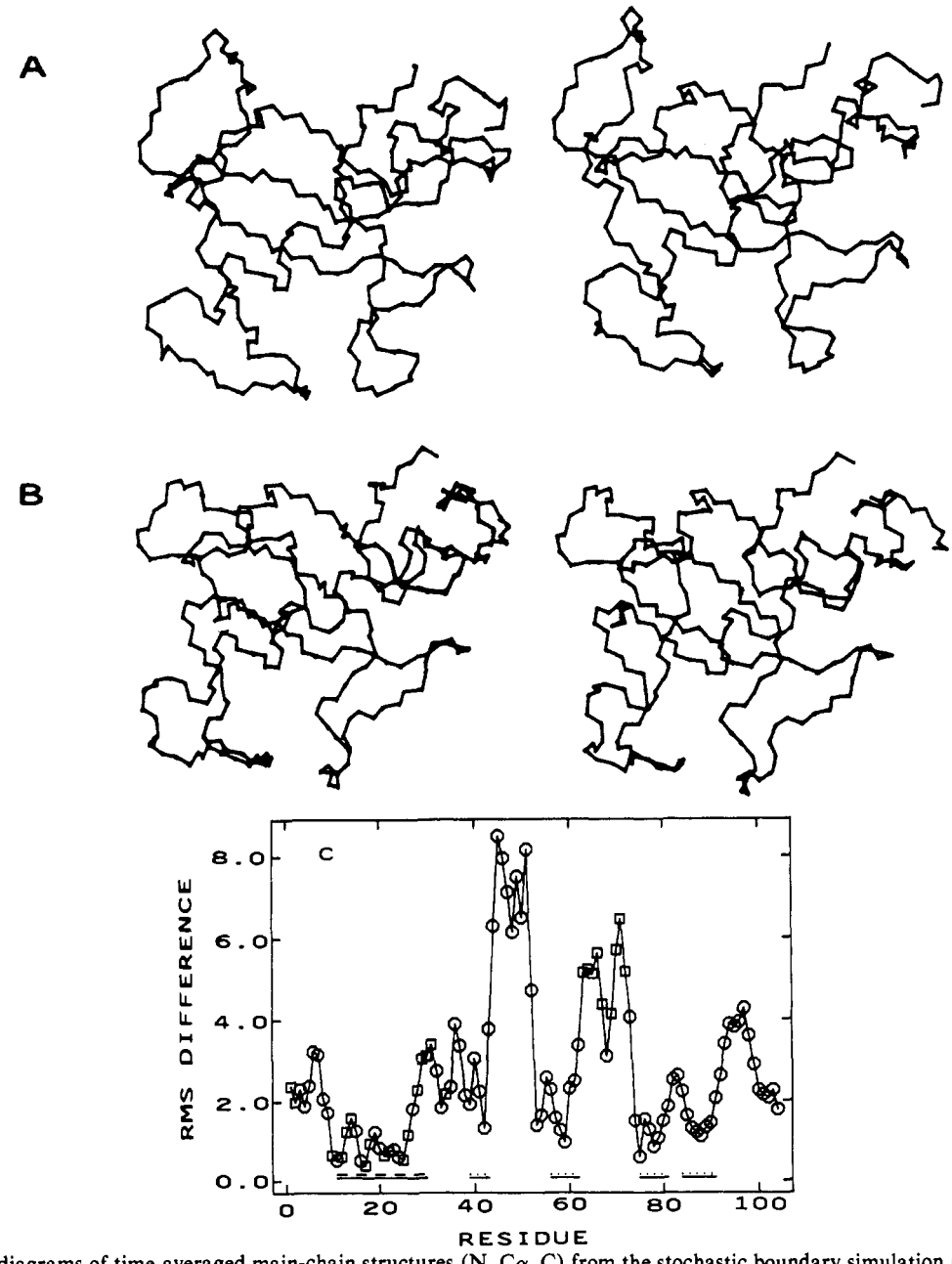


FIGURE 3: Stereo diagrams of time-averaged main-chain structures (N, Cα, C) from the stochastic boundary simulation (A) and the vacuum simulation (B). (C) RMS differences between time-averaged backbone atom (N, Cα, C, O) positions from the stochastic boundary and vacuum simulations. Residues in the α-helix are underscored with (---) and in the β-sheet with (...).

both cases there were initial structural changes during the minimization and initial portions of the trajectories. Comparison of panels A and B of Figure 2 shows the potential energy and RMS difference to relax in a similar fashion for the two simulations followed by approximately stable values, indicating that in both simulations energetically stable structures had been reached (Åqvist et al., 1986). With the SBS the RMS difference with the X-ray coordinates was much lower as compared to the VS, indicating the influence of water on the dynamically stable structures that were obtained (see below).

*Overall Structure.* Stereo representations of the main-chain atoms (N, Cα, C) from the time-averaged structures of both the SBS and VS are presented in panels A and B, respectively, of Figure 3, in a similar orientation to the diagrammatic representation of the structure in Figure 1A. Analysis of the stereo diagrams shows the two overall structures to be similar. Closer comparison of the differences in the backbone atoms (N, Cα, C, O) between the two MD time-averaged structures is presented in Figure 3C. Regions of secondary structure (α-helix, β-sheet) were quite similar for the two structures while the largest differences occurred in the loop regions. Two of these regions, including residues 43–52 and 93–99, are portions of the enzyme that directly interact with the guanine moiety of 2′GMP in the X-ray structure. Interestingly, of the two regions in which the largest differences occurred between the simulated structures, the 43–52 loop residues lie entirely in the 18-Å water ball in the SBS while loop region 63–74 is primarily outside the water ball in the Langevin region of the SBS simulation. Furthermore, comparison of the RMS differences for Langevin residues of the SBS showed a large variation, with small differences in the α-helix region as compared to larger differences in the loop 63–72 region. Thus, the presence of water in the SBS as well as leading to significant differences within the 18-Å water ball as compared to the VS also led to differences in the Langevin region.

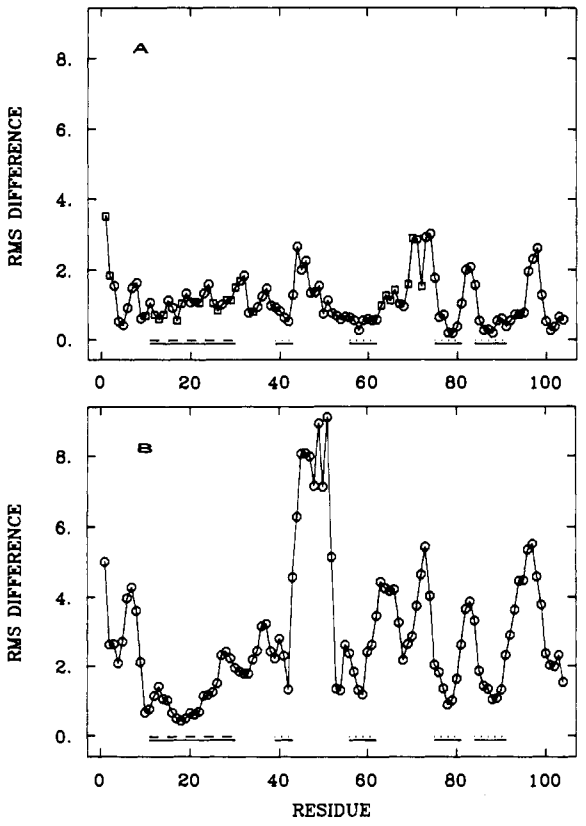


FIGURE 4: RMS differences between the time-averaged structures and the X-ray structure from the stochastic boundary simulation (A) and the vacuum simulation (B) for the backbone atoms (N, Cα, C, O). Residues represented by circles were subjected to the full MD dynamics while those represented by squares were subjected to Langevin dynamics. Residues in the α-helix are underscored with (---) and in the β-sheet with (...).

Presented in panels A and B of Figure 4 are the RMS differences between the time-averaged SBS and VS structures and the X-ray structure, respectively. As expected, the regions of secondary structure were quite similar in both cases, while large differences occurred in most of the loop regions. In the SBS structure (Figure 4A) significant differences were seen in regions that interact with the guanine of 2′GMP as well as at the N-terminal and the section between residues 69 and 75. A similar pattern also was observed in the VS structure (Figure 4B); however, the differences were much larger as compared to the SBS structure. These large differences between the VS and X-ray structures were primarily responsible for the differences observed between the two MD time-averaged structures (Figure 3C). Further MD studies on the 2′GMP–RNase T1 complex support the structural changes observed in this report and will be presented elsewhere (MacKerell et al., submitted for publication). The removal of 2′GMP from the enzyme, therefore, appeared to cause changes in the loop regions that interact with the guanine of 2′GMP, while the presence of water in the active-site region led to a damping of the changes observed.

*Overall Fluctuations.* RMS fluctuations for backbone and side-chain atoms for the SBS and VS are presented in Figure 5. The lowest RMS fluctuations were in the regions of secondary structure while the loop regions were much more flexible. Overall, for both the side-chain and backbone atoms, the majority of residues had larger fluctuations in the SBS as compared to the VS. This increased mobility was most significant for the residues in loop regions that interact directly with water molecules, implicating the presence of water to influence those motions (see below). Furthermore, an increased mobility also occurred in residues that lie in the interior of the protein, suggesting that the protein–water interactions occurring at the surface of the enzyme also influence motions in the protein interior.

Table I: RMS Differences between Time-Averaged Positions of Active-Site Residues and the Initial X-Ray Positions[a]

| | SBS | | VS | |
|---|---|---|---|---|
| residue | backbone | side chain | backbone | side chain |
| | | RS Region | | |
| 42 | 0.53 | 1.21 | 1.32 | 2.56 |
| 43 | 1.29 | 2.33 | 4.57 | 3.93 |
| 44 | 2.65 | 3.08 | 6.28 | 7.66 |
| 45 | 2.00 | 2.07 | 8.06 | 7.65 |
| 46 | 2.26 | 2.30 | 8.08 | 4.65 |
| 98 | 2.61 | 3.64 | 4.58 | 7.66 |
| | | CS Region | | |
| 40 | 0.83 | 1.92 | 2.79 | 3.60 |
| 58 | 0.26 | 1.54 | 1.30 | 2.25 |
| 77 | 0.72 | 2.41 | 1.35 | 3.03 |
| 92 | 0.55 | 1.69 | 2.89 | 2.74 |

[a] Values are in Å.

Table II: RMS Fluctuations of the Active-Site Residues[a]

| | SBS | | VS | |
|---|---|---|---|---|
| residue | backbone | side chain | backbone | side chain |
| | | RS Region | | |
| 42 | 0.74 | 0.82 | 0.39 | 0.41 |
| 43 | 0.78 | 1.11 | 0.43 | 0.84 |
| 44 | 0.81 | 1.04 | 0.45 | 0.52 |
| 45 | 0.87 | 1.27 | 0.47 | 0.49 |
| 46 | 1.10 | 1.29 | 0.47 | 0.46 |
| 98 | 1.30 | 2.11 | 0.57 | 0.74 |
| | | CS Region | | |
| 40 | 0.62 | 0.87 | 0.39 | 0.48 |
| 58 | 0.65 | 0.74 | 0.36 | 0.37 |
| 77 | 0.86 | 0.87 | 0.36 | 0.40 |
| 92 | 0.98 | 1.26 | 0.42 | 0.43 |

[a] Values are Å.

*Active-Site Structure.* Analysis of the active site can be simplified by dividing that region into two parts. The first region, designated RS, contains residues 42–46 and 98, which interact primarily with the guanine moiety of 2′GMP in the X-ray structure and represent the recognition site. The second region, which contains residues 40, 58, 77, and 92 and is designated CS, interacts primarily with the phosphate moiety of 2′GMP and is the catalytic site as determined by chemical modification and spectroscopic studies (Takahashi & Moore, 1982). Comparison of the RMS differences in Table I and fluctuations in Table II for these residues shows significant differences between the two simulations performed.

Analysis of the RMS differences between the RS residues from the MD time-averaged structures and the X-ray structure (Table I) showed a large difference between the residue positions in the two structures. This difference was much more pronounced in the VS structure (Table I), although significant differences also occurred in these regions of the SBS structure. Figure 6, which shows the time-averaged active-site structures for the two simulations, allows the actual structural differences to be observed. In both simulations hydrogen bonding between Glu-46 and the two tyrosines (42 and 45) sandwiching the guanosine in the crystal structure occurred (Table III). However, in the VS (Figure 6B) the RS residues collapsed into the empty active site, forming a series of residue–residue hydrogen bonds between RS and CS residues (Table III). An extreme change was seen in the position of the Tyr-45 side chain, which folded down into the CS region of the active site,

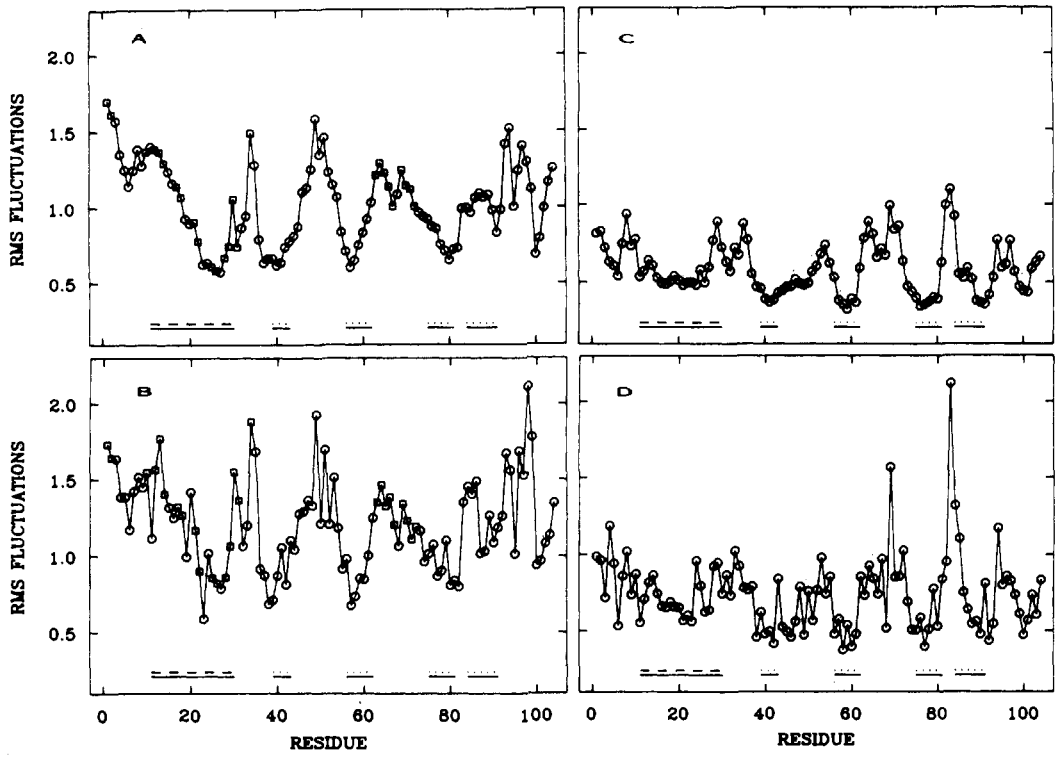


FIGURE 5: RMS fluctuations from the stochastic boundary simulation for the (A) backbone (N, Cα, C, O) and (B) side-chain (Gly O and not including hydrogens) atoms and from the vacuum simulation for the (C) backbone and (D) side-chain atoms. Residues in the α-helix are underscored with (---) and in the β-sheet with (...).

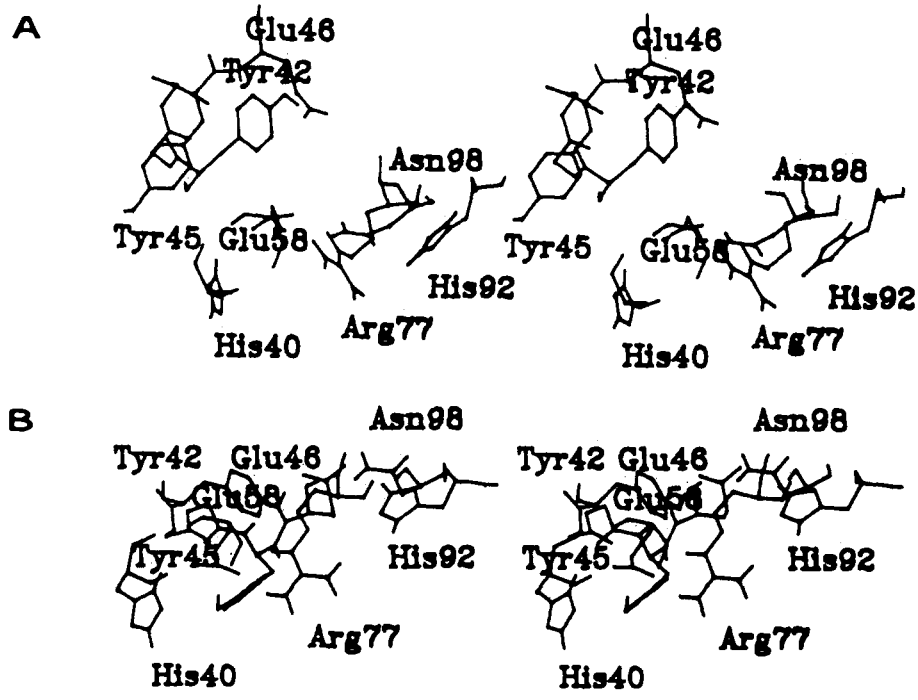


FIGURE 6: Stereo diagrams of the time-averaged positions of the active-site residues from the stochastic boundary simulation (A) and the vacuum simulation (B). The side chains of Asn-43 and Asn-44 are not present, and all waters were omitted from (A). Main-chain atoms from the time-averaged structures are in the same orientation.

with the Tyr-45 HH atom hydrogen bonding to Glu-58 Oε1 and Glu-53 Oε2. Glu-46 also moved down into the CS region, forming the hydrogen bond Glu-46 Oε1–His-92 Hε2. The combined positional changes of Tyr-45 and Glu-46, among others, apparently led to the large shift in the backbone atoms in the loop region 43–52 (Figure 4B). In contrast, the RS region in the SBS (Figure 6A) stayed open throughout the simulation, with only one hydrogen bond between the two regions occurring. The other hydrogen bonds were replaced by a number of protein–water hydrogen bonds (not shown) which prevented the protein–protein hydrogen bonds between RS and CS atoms seen in the VS from forming.

In the CS region of the active site the two MD time-averaged structures were more similar than in the RS region (Table I), although differences still occurred. Both structures contained a network of protein–protein hydrogen bonds (Figure 6, Table III) including the characteristic salt bridge triad His-40–Glu-58–Arg-77. However, with His-92 there were no

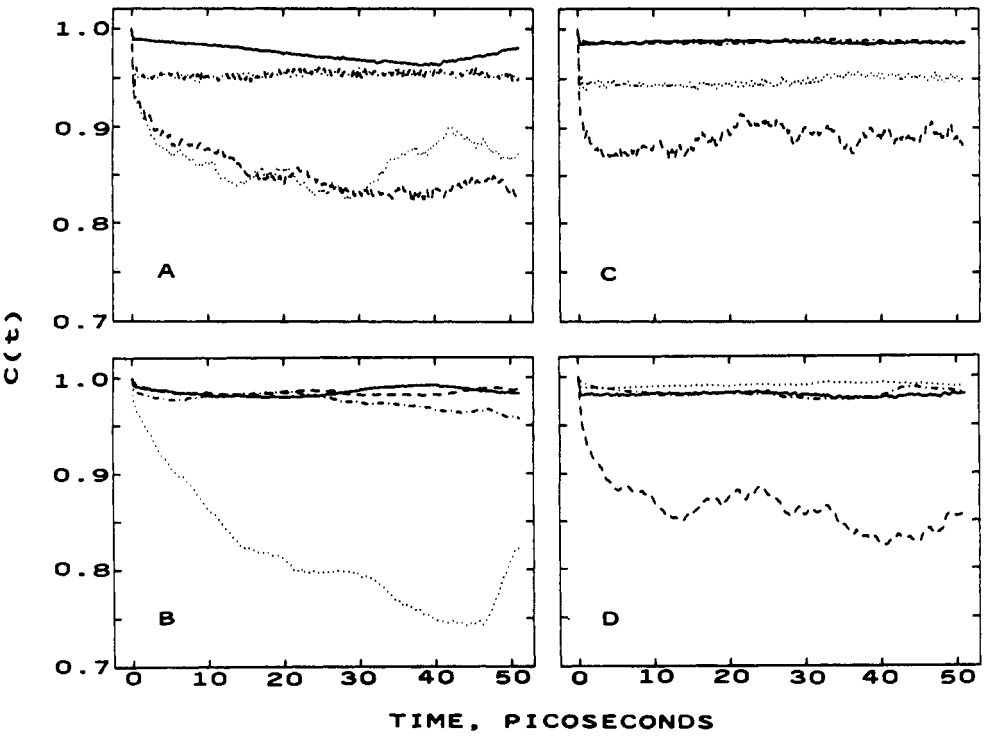


FIGURE 7: Time correlation functions of the Cδ1–Cδ2 (A and C) and Cγ–Cζ (B and D) vectors of the tyrosine side chain from the stochastic boundary (A and B) and the vacuum (C and D) simulations for tyrosines-11 (dot–dash), -24 (dash), -42 (line), and -45 (dot).

Table III: Comparison of Selected Hydrogen Bonds between Active-Site Residues in the Time-Averaged Simulation Structures[a]

| hydrogen bond | | distance (Å) | |
|---|---|---|---|
| donor | acceptor | SBS | VS |
| | RS Region | | |
| Tyr-42 HH | Glu-46 Oε2 | 2.0 | 2.0 |
| Tyr-45 H | Tyr-42 OH | | 2.1 |
| Glu-46 H | Glu-46 Oε2 | 2.1 | 2.5 |
| | CS Region | | |
| His-40 H | Glu-58 O | 2.1 | |
| Glu-58 H | His-40 O | 1.8 | 1.9 |
| His-40 Hδ1 | Glu-58 Oε1 | 2.0 | 2.2 |
| Arg-77 HH22 | Glu-58 Oε1 | 2.2 | |
| Arg-77 Hε | Glu-58 Oε2 | 2.2 | 2.1 |
| Arg-77 HH22 | Glu-58 Oε2 | 1.8 | 1.8 |
| | RS–CS | | |
| Asn-43 H | Glu-58 Oε1 | | 2.1 |
| Tyr-45 HH | Glu-58 Oε1 | | 2.1 |
| Tyr-45 HH | Glu-58 Oε2 | | 2.3 |
| His-92 Hε2 | Asn-98 Oδ1 | 1.9 | |
| His-92 Hε2 | Asn-98 O | | 2.0 |
| His-92 Hε2 | Glu-46 Oε1 | | 2.1 |

[a] Selected hydrogen bonds between recognition site residues (RS), catalytic site residues (CS), and residues in the recognition site and catalytic site (RS–CS) following 120 steps of adopted-basis Newton Raphson minimization of the protein atom time-averaged coordinates. Criteria for hydrogen bond existence are hydrogen–acceptor distance <3.0 Å and donor–hydrogen–acceptor angle <65°.

protein–protein hydrogen bonds with other CS residues. Instead, the residue hydrogen bonded to RS residues and, for the SBS, was surrounded by water molecules (not shown). Another change of interest was the hydrogen bonding between the backbone atoms of His-40 and Glu-58. In the SBS structure both His-40 H–Glu-58 O and His-40 O–Glu-58 H hydrogen bonds were present while only the His-40 H–Glu-58 O bond was present in the VS structure. These two hydrogen bonds would help to maintain the orientation of the two residues which are possibly involved in a proton-transfer complex in the catalytic mechanism. Thus, in contrast to the RS region of the active site, the structure of the CS region is somewhat maintained in the two simulations. This structural rigidity is probably attributable to residues 40, 58, and 77 being located on the β-pleated sheet while His-92, where the hydrogen bonds are not conserved, is just at the end of a β-strand in a loop region. Stabilization of His-40 and Glu-58 is probably also increased by the presence of prolines-39 and -60, which are highly conserved in ribonucleases of the T1 family (Hill et al., 1983).

Table II shows the values of the RMS fluctuations of the RS and CS residues. As may be seen, the fluctuations were larger in the SBS than in the VS active-site residues. This greater mobility in the SBS again appears to be due to an absence of strong protein–protein interactions which led to both the large structural changes and lowered mobility in the VS. These differences further point to the importance of water in the simulation concerning both structural changes and dynamics of the enzyme. Furthermore, the motions in the active site, especially in the RS region, are probably of importance for the binding of substrates or inhibitors to the enzyme, possibly causing "open" states to which binding may occur. In depth analysis of the effect of water on specific hydrogen bonds in the simulations is currently under investigation.

Of special interest in the RS portion of the active site is the motion of the two tyrosine residues (42 and 45) which form a stacked complex with the guanine base of 2′GMP. To understand the influence of water on their motions, time correlation functions $C(\tau)$ for vectors through the side-chain atoms Cδ1–Cδ2 and Cγ–Cζ were calculated by using

$$C(\tau) = \langle \hat{\mathbf{Q}}(t) \cdot \hat{\mathbf{Q}}(t+\tau) \rangle \qquad (3)$$

where $\hat{\mathbf{Q}}(t)$ is the normalized vector of interest at time $t$, $\tau$ is a varying time increment, and the broken brackets ($\langle\ \rangle$) indicate time averaging. Results presented in Figure 7 show the time correlations for Tyr-11, -24, -42 and -45 for the Cδ1–Cδ2 (Figure 7A,C) and the Cγ–Cζ vectors (Figure 7B,D) for the SBS and VS, respectively. Tyrosines-11 and -24 were also included due to their positions being removed from the active

site. Results for the two active-site tyrosines showed significant differences. Tyr-42 was quite immobile in both simulations, although more so in the VS (Table II). This was apparently due to Tyr-42 being part of the $\beta$-sheet, the hydrogen bonding of Tyr-42 OH and HH (Table III), and the residue lying at the bottom of the recognition site where it is surrounded by hydrophobic residues including Phe-48, Phe-50, Tyr-56, Val-79, Ile-90, and Phe-100. Furthermore, the primarily hydrophobic environment of Tyr-42 probably minimized the direct effect of solvent on its motion. In contrast, Tyr-45 lies on the surface of the protein, allowing direct interaction with the solvent. Examination of Figure 7 shows that the presence of water greatly increased the motion of Tyr-45 for both vectors analyzed. This difference was due to Tyr-45 folding down into the CS region of the active site and hydrogen bonding to Glu-58 (Figure 6B, Table III) in the VS while the residue was surrounded by water and free to move in the SBS. Tyr-11 lies in a hydrophobic cleft surrounded by residues Asn-9, Val-16, Ile-61, Asp-76 and Val-89, similar to the environment of Tyr-42. Again, there was only a small difference in the motion of that residue in the SBS as compared to the VS, due to its hydrophobic environment and a hydrogen bond between Tyr-11 HH and Asp-76 O$\delta$2. Lastely, Tyr-24, which lies on the protein surface and is one of the $\alpha$-helix residues, showed a significant mobility in the VS. This increased mobility appears to be due to the residue lying adjacent to the loop 81–84 which is also highly mobile in the VS (Figure 5). Apparently, the presence of a few bound water molecules in this region, which were included in the simulation in locations known from the crystal structure, allowed for more favorable interactions which led to a lower mobility in the SBS as compared to the VS. Thus, the presence of water in the SBS led to only a small increase in the motion of tyrosines-11 and -42, which are less exposed to solvent while the influence was much greater for the exposed tyrosines, with the mobility increased for Tyr-45 and decreased for Tyr-24. Overall, comparison of the RMS fluctuations in the SBS versus the VS (Figure 5), along with the increased mobility of the active-site residues (Table II) and the tyrosine motions (Figure 7), reveals a trend where an increased mobility was observed in the SBS, although exceptions do exist, especially with residues 24 and 81–84.

*Tryptophan-59 Motion.* Time-resolved fluorescence depolarization measurements have previously shown there to be a motion of Trp-59 occurring on a time scale of 100 ps (MacKerell et al., 1987a,b) which is also observed in a simulation of free RNase T1. In Figure 8 the second Legendre polynomial of the cross-correlation between the tryptophan side-chain absorption vector (−38° to the long axis) and emission vectors (±23° from the absorption vector) (Ichiye & Karplus, 1983) is presented for the two simulations. For both simulations the decays were similar, with an initial fast portion followed by a slower decay. However, the direction of the motion was different for the two as indicated by the −15° emission vector decreasing in the VS and the −61° emission vector decreasing in the SBS. Determination of the correlation times for the decays to compare with experimental data was done by assuming the presence of two uncoupled relaxation processes of limited amplitude, associated with the internal motion of Trp-59, and by using

$$r(t) = r_0(1 - P_\infty^1)e^{-t/\theta_1} + r_0P_\infty^1(1 - P_\infty^2)e^{-t/\theta_2} + r_0P_\infty^1P_\infty^2e^{-t/\theta_m} \quad (4)$$

where $r_0$ is the zero-time anisotropy, $P_\infty^1$ and $P_\infty^2$ are the plateau values of the correlation function for the fast relaxation processes with correlation times of $\theta_1$ and $\theta_2$, $t$ is the time, and

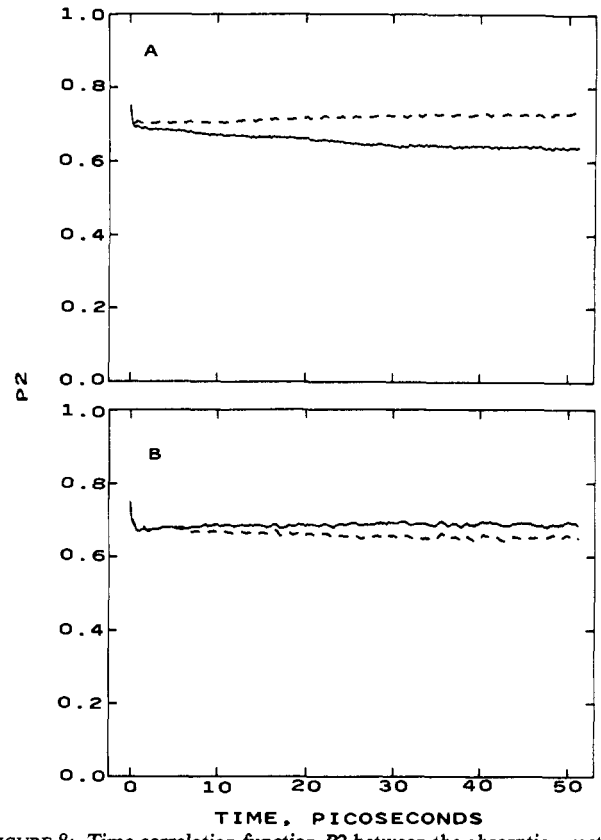


FIGURE 8: Time correlation function $P2$ between the absorption vector at −38° and emission vectors at −15° (---) and −61° (—) to the long axis of the Trp-59 side chain for the stochastic boundary (A) and vacuum (B) simulations.

$\theta_m$ is the relaxation time for the overall rotation of the protein. The value of $r_0$ is assumed to equal 0.31, corresponding to an angle of ±23° between the tryptophan absorption and emission vectors (Valeur & Weber, 1977). Since overall rotation of the protein was not present in the simulation, the last term on the right-hand side of eq 4 was treated as a constant. Rearrangement of eq 4 yields

$$r(t) - r_0P_\infty^1P_\infty^2 = r_0(1 - P_\infty^1)e^{-t/\theta_1} + r_0P_\infty^1(1 - P_\infty^2)e^{-t/\theta_2} \quad (5)$$

The relaxation time, $\theta_2$, for the slower decay (Figure 8) was determined from the slope of the outer linear portion of a plot of ln $[r(t) - r_0P_\infty^1P_\infty^2]$ versus $t$, using the minimum value of $\langle P2\rangle$ in Figure 8 as $r_0P_\infty^1P_\infty^2$. Analysis of the initial portion of the decay associated with $\theta_1$ was omitted due to the time range being experimentally unobservable. This treatment yielded values for $\theta_2$ of 39 ps for the SBS and 22 ps for the VS. It should be emphasized that the calculated $\theta_2$ values are dependent on the value of $r_0P_\infty^1P_\infty^2$, which have been determined by assuming that the decays in Figure 8 have reached their minimum values. The present model is well suited for a limited rotation associated with $\theta_2$ and is more physically realistic than the model previously used where the relaxation process associated with $\theta_2$ was assumed to reach a plateau value of zero (MacKerell et al., 1987b). Thus, although the present calculated values of $\theta_2$ are in worse agreement with the experimental correlation time of 100 ps at 313 K (MacKerell et al., 1987a,b) as compared to the previously reported simulation value of 130 ps, the agreement between the experimental and theoretical results may still be considered quite reasonable. Potential problems contributing to the disagreement include the truncation of electrostatic interactions, the lack of a full solvent representation, and the extremely limited sample size as well as possible error in the experimentally determined decay

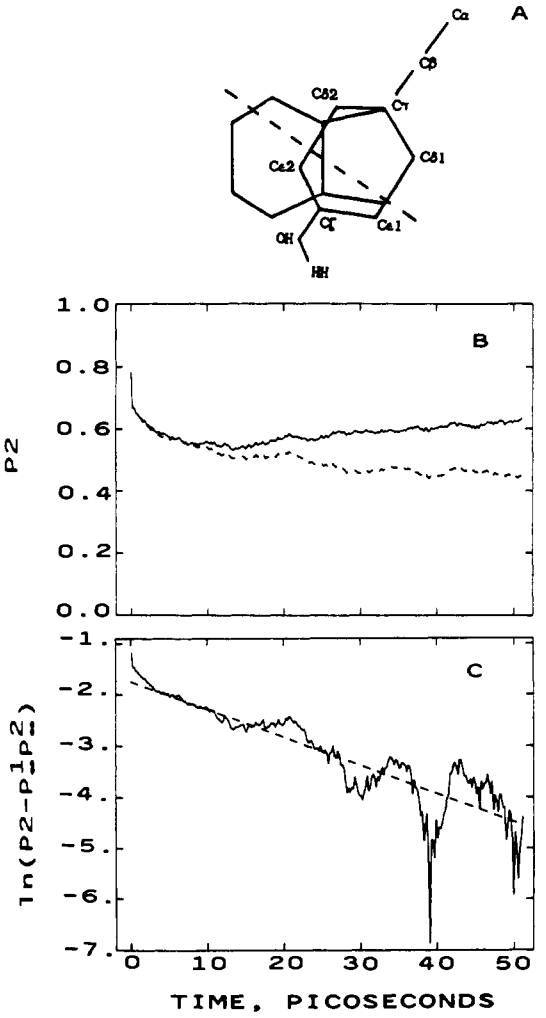


FIGURE 9: (A) Orientation of Cα–Cβ–Cγ–Cδ1 dihedral angles of tyrosine and tryptophan with the tryptophan $L_a^1$ absorption vector (−38°) (dashed line). Tyrosine atoms are labeled. Adapted from Yamamoto and Tanaka (1972). (B) Time correlation function $P2$ between the hypothetical absorption vector and emission vectors at +23° (—) and −23° (---) to the absorption vectors in tyrosine-45. (C) Logarithmic plot of the time correlation function $P2$ in panel B at −23°. Dashed line is the slope from which the correlation time was calculated. Note: The $y$ axis is represented as ln $(P2 - P_\infty^1 P_\infty^2)$ rather than ln $[r(t) - r_0 P_\infty^1 P_\infty^2]$ as shown in eq 4 and 5.

time. Analysis of the nature of the Trp-59 motion associated with $\theta_2$ in the simulations will be presented elsewhere.

Along with predicting a structure and dynamical fluctuations for the free enzyme form of RNase T1, the results may also be used to predict the results for time-resolved fluorescence depolarization measurements. Currently the ability exists to produce RNase T1 mutants, which will be used to produce an enzyme where Tyr-45 and Trp-59 are switched in the sequence (Hahn et al., unpublished results). By making the first-order approximation that a tryptophan at position 45 will move in a similar fashion to Tyr-45, we can predict the results of depolarization measurements on the above mutant. First, we assume that the Cα–Cβ–Cγ–Cδ1 dihedral angle is the same in both cases. This alignment then allows the designation of a hypothetical absorption vector in Tyr-45 lying across the phenyl ring, as shown in Figure 9A, which corresponds to the $L_a^1$ absorption vector in tryptophan which is the sole absorber for excitation at 300 nm (Valeur & Weber, 1977). The correlation functions, $\langle P2 \rangle$, were calculated by using this absorption vector and emission vectors at ±23° to the absorption vector. Results of this treatment of the SBS are presented in Figure 9B, showing a fast initial decay followed by a slower decay for both emission vectors. The decay associated with the −23° vector, which continues to decay, was treated by using eq 3 and a value of 0.437 for $P_\infty^1 P_\infty^2$ (minimum value in Figure 9B). This resulted in a $\theta_2$ value of 17 ps and a $P_\infty^1$ value of 0.663. Thus, in the experiments one would expect to see a fast decay in the time range of 100 ps or less with a zero-time anisotropy ($r_{0,\text{total}}$) of approximately 0.26 and an amplitude of 0.13 associated with the fast portion of the decay ($r_{0,1}$), when a true $r_0$ of 0.31 is assumed in eq 3.

## Conclusion

The results presented in this report indicated the occurrence of structural changes in RNase T1 upon the removal of the inhibitor 2′GMP, which were most prominent in regions of the protein that interact directly with the inhibitor in the crystal structure (Figures 3 and 4). The presence of water in the active-site region of RNase T1 influenced both the active-site geometries (Figure 5 and Table I) and overall structures (Figure 3), which may partially be due to the use of full charges in the vacuum simulation. This influence both agrees (Ahlström et al., 1987) and disagrees (Åqvist et al., 1986; M. Levitt, personal communication) with previous work indicating that the effect of water on the molecular structure may vary from protein to protein depending on its chain folding and amino acid sequence.

Water in the SBS also had a large influence on the fluctuations that were observed in RNase T1. In general, the presence of solvent increased the mobility of both backbone and side-chain atoms (Table II and Figures 5 and 7). This appears to be due to competition by water molecules for residue–residue interactions at the enzyme surface which readily occur in vacuum (Table III). An increased mobility was also observed in residues not directly exposed to the solvent. This implicated the transmission of surface effects to the protein interior, which is likely to be important in functional terms. The increased mobility of Tyr-45 (Figure 7) as well as of other side chains and of the backbone atoms in the recognition region of the active site (Table II) is probably important for producing an "open" recognition cavity in the enzyme to which an inhibitor or substrate can bind, whereas the lack of these motions in vacuo make such interactions much more difficult to visualize. Lastly, the results allowed for the prediction of the anisotropic decay of a theoretical tryptophan at position 45 which may ultimately be tested by using a site-specific mutant of RNase T1 and time-resolved fluorescence depolarization experiments.

## Acknowledgments

We are grateful to Thore Olausson and the Department of Medical Information Processing, Karolinska Institutet, for assistance with and use of the NORD-500 computer.

**Registry No.** RNase T1, 9026-12-4.

## References

Adelman, S. A. (1980) *J. Chem. Phys. 73*, 3145.

Ahlström, P., Teleman, O., Jönsson, B., & Forsen, S. (1987) *J. Am. Chem. Soc. 109*, 1541.

Åqvist, J., Sandblom, P., Jones, T. A., Newcomer, M. E., van Gunsteren, W. F., & Tapia, O. (1986) *J. Mol. Biol. 192*, 593.

Arata, Y., Kimura, S., Matsuo, H., & Narita, K. (1979) *Biochemistry 18*, 18.

Arni et al. (1988) *J. Biol. Chem.* (submitted for publication).

Belch, A. C., & Berkowitz, M. (1985) *Chem. Phys. Lett. 113*, 278.

Berkowitz, M., & McCammon, J. A. (1982) *Chem. Phys. Lett. 80*, 215.
Brooks, B., Bruccoleri, R., Olafson, O., States, D. J., Swaminathan, S., & Karplus, M. (1983) *J. Comput. Chem. 4*, 187.
Brooks, C. L., & Karplus, M. (1983) *J. Chem. Phys. 79*, 6312.
Brooks, C. L., Brunger, A., & Karplus, M. (1985) *Biopolymers 24*, 843.
Brunger, A., Brooks, C. L., & Karplus, M. (1984) *Chem. Phys. Lett. 105*, 495.
Brunger, A., Brooks, C. L., & Karplus, M. (1985) *Proc. Natl. Acad. Sci. U.S.A. 82*, 8458.
Egami, F., Takahashi, K., & Uchida, T. (1964) *Prog. Nucleic Acid Res. Mol. Biol. 3*, 59.
Hagler, A. T., & Moult, J. (1978) *Nature (London) 272*, 222.
Heinemann, U., & Saenger, W. (1982) *Nature (London) 299*, 27.
Hill, C., Dodson, G., Heinemann, U., Saenger, W., Mitsui, Y., Nakamura, K., Borisow, S., Tischenko, G., Polyakov, K., & Pavlosvky, S. (1983) *Trends Biochem. Sci. (Pers. Ed.) 8*, 364.
Ichiye, T., & Karplus, M. (1983) *Biochemistry 22*, 2884.
Jorgensen, W. L., Chandrasekar, J., Madura, J. D., Impey, R. W., & Klein, M. L. (1983) *J. Chem. Phys. 79*, 926.
Karplus, M., & McCammon, J. A. (1981) *CRC Crit. Rev. Biochem. 9*, 293.
Levy, R. M., Sheridan, R. P., Keepers, J. W., Dubey, G. S., Swaminathan, S., & Karplus, M. (1985) *Biophys. J. 48*, 509.
MacKerell, A. D., Jr., Rigler, R., Hahn, U., & Saenger, W. (1987a) in *Structure, Dynamics and Function of Biomolecules* (Ehrenberg, A., Rigler, R., Gräslund, A., & Nilsson, L., Eds.) Springer Series in Biophysics, Vol. 1, p 260, Springer-Verlag, Berlin.
MacKerell, A. D., Jr., Rigler, R., Nilsson, L., Hahn, U., & Saenger, W. (1987b) *Biophys. Chem. 26*, 247.
Martin, P. D., Tulinsky, A., & Walz, F. G., Jr. (1980) *J. Mol. Biol. 136*, 95.
McCammon, J. A. (1984) *Rep. Prog. Phys. 47*, 1.
McCammon, J. A., & Harvey, S. C. (1987) *Dynamics of Proteins and Nucleic Acids*, Cambridge University Press, London.
Palmer, R. G. (1982) *Adv. Phys. 31*, 669.
Reiher, W. E. ((1985) Ph.D. Thesis, Harvard University, Cambridge, MA.
Roberts, G. C. K., Dennis, E. A., Meadows, D. H., Cohen, J. S., & Jardetzky, O. (1969) *Proc. Natl. Acad. Sci. U.S.A. 62*, 1151.
Ruterjans, H., & Pongs, O. (1971) *Eur. J. Biochem. 18*, 313.
Ryckaert, J. P., Ciccotti, G., & Berendsen, H. J. C. (1977) *J. Comput. Phys. 23*, 327.
Steitz, T. A., Harrison, R., Weber, I. T., & Leahy, M. (1982) in *Mobility and Function in Proteins and Nucleic Acids, CIBA Foundation Symposium 93*, p 25, Pitman, London.
Sugio, S., Anisak, T., Ohishi, H., Tomita, K. I., Heinemann, U., & Saenger, W. (1985a) *FEBS Lett. 181*, 129.
Sugio, S., Anisak, T., Ohishi, H., Tomita, K. I., & Saenger, W. (1985b) *FEBS Lett. 183*, 115.
Takahashi, K., & Moore, S. (1982) *Enzymes (3rd Ed.) 13*, 435.
Uchida, T., & Egami, F. (1971) *Enzymes (3rd Ed.) 4*, 205.
Valeur, B., & Weber, G. (1977) *Photochem. Photobiol. 25*, 441.
van Gunsteren, W. F., & Karplus, M. (1982) *Macromolecules 15*, 1528.
Warshel, A. (1979) *J. Phys. Chem. 83*, 1640.
Warshel, A. (1984) *Proc. Natl. Acad. Sci. U.S.A. 81*, 444.
Warshel, A., & Levitt, M. (1976) *J. Mol. Biol. 103*, 227.
Warshel, A., & Russell, S. T. (1984) *Q. Rev. Biophys. 17*, 283.
Yamamoto, Y., & Tanaka, J. (1972) *Bull. Chem. Soc. Jpn. 45*, 1362.